Molecular basis for stereoselective transport of fenoterol by the organic cation transporters 1 and 2

Lukas Gebauer [a], N. Arul Murugan [b], Ole Jensen [a], Jürgen Brockmöller [a], Muhammad Rafehi [a,*]

[a] *Institute of Clinical Pharmacology, University Medical Center Göttingen, 37075 Göttingen, Germany*
[b] *Department of Computer Science, School of Electrical Engineering and Computer Science, KTH Royal Institute of Technology, S-10044 Stockholm, Sweden*

1. Introduction

Stereoselectivity in drug membrane transport has only received minor attention, despite the fact that many drugs currently on the market have chiral centres and that stereoselectivity is most important in other pharmacological processes, including receptor binding and drug metabolism [1,2]. The action of the majority of racemic drugs relies on one bioactive enantiomer (the eutomer), while the other enantiomer (the distomer) may cause off-target effects and drug-interactions [2]. Consequently, any unequal membrane transport can shift the risk-benefit-ratio of a racemic drug into either a beneficial or an unfavourable direction. Therefore, stereoselective pharmacokinetics can have substantial effects on the effectiveness and safety of drug therapy.

Organic cation transporters (OCTs) of the solute carrier (SLC) 22 family mediate the cellular uptake of a wide array of cationic drugs, metabolites, toxins, and other endogenous and exogenous compounds [3]. OCT1 (*SLC22A1*) is mainly expressed at the basolateral membrane of hepatocytes [3,4], whereas OCT2 (*SLC22A2*) is located in the basolateral membrane of epithelial cells in the proximal tubules of the kidney [3,5]. These two transporters mediate the uptake of a number of drugs in liver and kidney as prerequisite for metabolism and excretion and thereby determine their pharmacokinetics. For example, the systemic exposure to fenoterol, a β_2-adrenergic receptor agonist used for bronchodilation in the treatment of asthma, was almost twice as high in carriers of heritable OCT1 deficiency compared to carriers of fully active OCT1 [6], which demonstrates the role of OCT1 in the pharmacokinetics

Abbreviations: 3D, three-dimensional; Cl_{int}, intrinsic clearance; DMEM, Dulbecco's modified Eagle's medium; FCS, foetal calf serum; HBSS, Hank's balanced salt solution; HEK, human embryonic kidney; HPLC-MS/MS, high performance liquid chromatography tandem mass spectrometry; OCT, organic cation transporter; PCR, polymerase chain reaction; rt, room temperature; SLC, solute carrier; v_{max}, maximum transport velocity; WT, wild-type.

* Corresponding author at: Institute of Clinical Pharmacology, University Medical Center Göttingen, Robert-Koch-Str. 40, 37075 Göttingen, Germany.
E-mail address: Muhammad.rafehi@med.uni-goettingen.de (M. Rafehi).

Table 1
PCR primers used for the generation and validation of mutated OCT1 and OCT2 cell lines (purchased from Sigma-Aldrich, Darmstadt, Germany).

Site-directed mutagenesis primers

Transporter	Mutation	Direction	Sequence (5′-3′)[a]
OCT1	F355A	Forward	CCTGATGTACCTGTGG**GC**CACGGACTCTGTGCTC
		Reverse	GAGCACAGAGTCCGTG**GC**CCACAGGTACATCAGG
	N410A	Forward	CCCCATGGCCATGTCA**GC**TTTGTTGGCGGGGGCAGCC
		Reverse	GGCTGCCCCCGCCAACAAA**GC**TGACATGGCCATGGGG
	I442A	Forward	GTTGGCCGAATGGGA**GC**CACCATTGCAATACAAATG
		Reverse	CATTTGTATTGCAATGGT**GC**TCCCATTCGGCCAAC
	F244A	Forward	CATGTACCAGATGGCC**GC**CACGGTGGGGCTGGTGG
		Reverse	CCACCAGCCCCACCGTG**GC**GGCCATCTGGTACATG
	T272A	Forward	GGCAGTCTCCCTGCCC**GC**CTTCCTCTTCCTGCTC
		Reverse	GAGCAGGAAGAGGAAG**GC**GGGCAGGGAGACTGCC
OCT2	L438A	Forward	GGCTAAAAATTATTATCTCATGC**GC**GGAAGAATGGGGATC
		Reverse	GATCCCCATTCTTCCC**GC**GCATGAGATAATAATTTTTAGCC
	T246A	Forward	CCAAGTTGCCTAT**GC**AGTTGGGCTCCTGGTGC
		Reverse	GCACCAGGAGCCCAAC**TGC**ATAGGCAACTTGG

Validation PCR primers

Reaction	Primer	Sequence (5′-3′)	Amplicon size [bp]
Integration PCR	P_{SV40}	AGCTGTGGAATGTGTGTCAGTTAGG	519
	P_{Hyg_r2}	ACGCCCTCCTACATCGAAGCTGAAA	
Multiple integration PCR	P_{FRT_f}	AATCGGGGGCTCCCTTTAGGGTTCC	273
	P_{Hyg_r2}	ACGCCCTCCTACATCGAAGCTGAAA	
	P_{OCT2_r}	CAGGTAGATATTGTCACCTGC	

Quantitative real-time PCR primers

Gene	Direction	Sequence (5′-3′)	Amplicon size [bp]
HPRT1	Forward	TGACACTGGCAAAACAATGCA	94
	Reverse	GGTCCTTTTCACCAGCAAGCT	
OCT1	Forward	TGTCACCGAAAAGCTGAGCC	96
	Reverse	TCCGTGAACCACAGGTACATC	
OCT2	Forward	ATGTACAACTGGTTCACGAG	81
	Reverse	CAGGTAGATATTGTCACCTGC	

[a] Affected codons are underlined and the substituted nucleobases are highlighted in bold.

of fenoterol.

Recently, we have studied the extent of stereoselectivity in the cell uptake of adrenergic agonists and antagonists by OCT1, OCT2, and related transporters [7]. Most notably, fenoterol was transported in a stereoselective manner by OCT1 and OCT2 but with opposite enantiopreference: OCT1 showed a 2-fold higher maximum transport velocity (v_{max}) for the eutomer (*R,R*)-fenoterol, while OCT2 displayed a 20-fold higher v_{max} for the distomer (*S,S*)-fenoterol [7]. Stereoselective effects were observed for some of the other tested adrenergic and anti-adrenergic drugs as well, but given the opposite enantiopreference between OCT1 and OCT2 and the 10-fold difference therein, fenoterol was most interesting and thus chosen for further studies. The reasons for the strong differences between these two closely related (70% sequence homology) transporters are not clear, as a general understanding of the underlying molecular mechanisms of transporter-enantiomer interactions is still lacking. In fact, stereoselective effects might not have been expected altogether in light of the very broad substrate profiles of OCT1 and OCT2.

A pharmacophore model previously developed for studying stereoselective binding of chiral drugs to OCT1 was composed of a positive charge as well as a hydrophobic and two hydrogen-bond acceptor sites [8]. When mapping (*R,R*)- and (*S,S*)-fenoterol to this model, only the positive interaction site and both hydrogen-bond acceptor sites were found to be essential for binding. However, for the highly polymorphic OCT1, genetic variation leading to the substitution of a single or merely a few amino acids can have strongly reduced transporter function [9]. Moreover, site-directed mutagenesis studies indicated that multiple binding sites may contribute to substrate recognition and translocation, and might therefore also play a role in transporter stereoselectivity [10,11].

In the absence of experimentally-derived three-dimensional (3D) structures for either OCT1 or OCT2, an alternative approach to studying stereospecific recognition and molecular interaction between these transporters and their ligands is through homology modelling. Several 3D structures for human OCT1 generated using homology modelling have been reported. These models were based on the X-ray diffraction structures of the high-affinity phosphate transporter from *Serendipita indica* [12], the human glucose transporter 3 [13], or the glycerol-3-phosphate transporter from *Escherichia coli* [14]. The sequence identities between these template proteins and human OCT1 is around 20%. With respect to OCT2, a homology model was based on the same structure of the glycerol-3-phosphate transporter [15].

In order to explore the binding interactions between OCT1 and OCT2 with fenoterol and find a possible explanation for the opposing enantiopreference, novel homology models for human OCT1 and OCT2 were constructed. These were based on the X-ray diffraction structure of sugar transporter 10 of *Arabidopsis thaliana*, which shows the transporter in an outward occluded conformation at a resolution of 2.4 Å [16]. Computational docking and molecular dynamics simulations of (*R,R*)-fenoterol and (*S,S*)-fenoterol in the putative substrate binding sites was done to identify possible residues that strongly interact with each enantiomer. These were subsequently replaced by alanine through site-directed mutagenesis and the effects of these substitutions on the transport kinetics of both fenoterol enantiomers in both transporters were studied in vitro. This provided experimental data for the validation of the homology models and to support our hypotheses on the molecular interactions between OCT1 and OCT2 with fenoterol.

Table 2
Mass spectrometry detection parameters.

Compound	Retention time [min]	Mass Q1[a] [Da]	Mass Q3[b] [Da]	DP[c] [V]	CE[d] [V]	CXP[e] [V]
Aciclovir	3.77	225.9	151.9	46	17	10
			(134.9)	(46)	(40)	(8)
Fenoterol	3.71 / 4.86	304.1	107.1	70	44	12
			(135.2)	(70)	(24)	(12)
Fenoterol-d6	3.71 / 4.86	310.3	109.1	70	40	12
				(70)	(26)	(12)
			(141.0)			
Salbutamol	6.25 / 7.02	240.2	222.2	60	24	15
			(148.2)	(60)	(24)	(15)

Detection parameters for a second compound-specific mass transition used as qualifier are shown in parentheses.
[a]Q1, first quadrupole
[b]Q3, third quadrupole
[c]DP, declustering potential
[d]CE, collision energy
[e]CXP, collision cell exit potential

2. Materials and methods

2.1. Development of OCT1 and OCT2 homology models

To study the binding of fenoterol (both its (*R,R*)- and (*S,S*)-enantiomers) to OCT1 and OCT2, the 3D structures of these transporters are required. Since experimentally-derived structures are not available, homology modelling was carried out for these two human uptake transport proteins using the online server SWISSMODEL [17]. The sequence details for human OCT1 and OCT2 were obtained from the UniProt knowledge database [18]; the UniProt IDs for OCT1 and OCT2 are O15245 and O15244, respectively. The 3D structure of Sugar Transport Protein 10 of *Arabidopsis thaliana*, obtained from the Protein Data Bank (PDB ID 6H7D), was used as the template [16,19]. This structure is at a resolution of 2.40 Å and shows the protein in an outward occluded state in complex with glucose. The sequence identities between either OCT1 or OCT2 and this template is approximately 20%, which is similar to the previously published homology models [12–15], as no more closely related template structures with a resolution below 2.5 Å could be found. Given the high flexibility of the N-terminal loop, the first 134 (for OCT1) and 142 (for OCT2) residues could not be included in our homology models.

2.2. Computational docking, molecular dynamics simulations, and binding free energy calculations

The 3D structures for OCT1 and OCT2, obtained through homology modelling, were used for molecular docking studies using AutoDock Vina [20]. The molecular structures were built using Molden software [21,22]. Their geometries were optimised by employing density functional theory at B3LYP-level and 6-31G* basis set using Gaussian 09 [23]. Using Open Babel [24] and MGLTools [25,26], Gaussian output files were converted to .mol2- and .pdbqt-files, respectively. The .pdbqt-files were used as input for molecular docking. The gridbox was defined to include the sugar binding site as in the template structure and with 64 grid points each along the x-, y-, and z-directions. The default grid spacing used was 0.375 Å. Twenty low energy binding modes were stored. Multiple binding sites and binding modes were identified for both fenoterol enantiomers in both OCT1 and OCT2, and these were

Table 3
Binding free energies for (*R,R*)- and (*S,S*)-fenoterol in OCT1 and OCT2.

	Binding free energy [kcal/mol]	
	OCT1	OCT2
(*R,R*)-fenoterol	−38.2	−15.5
(*S,S*)-fenoterol	−25.9 (−19.3 for OCT1_F244A_T272A)	−30.0

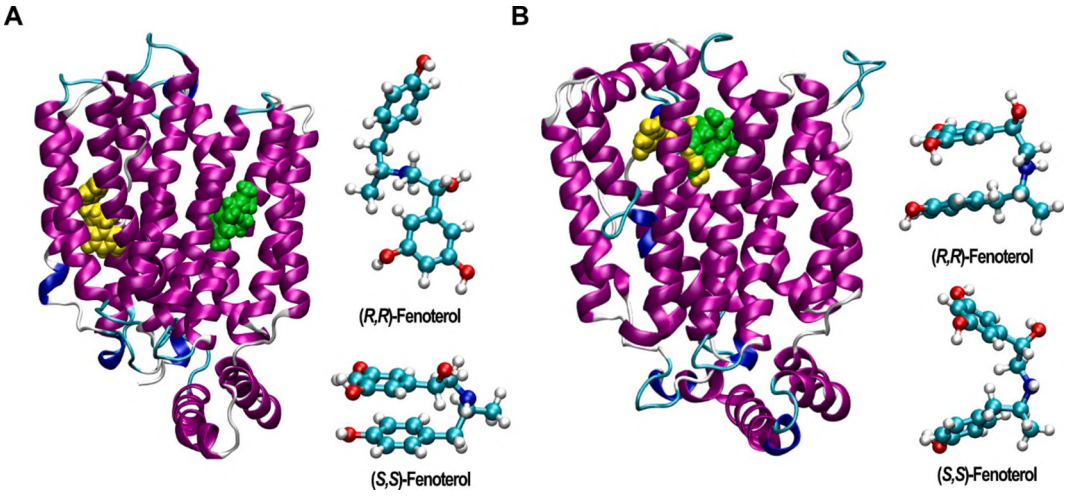

Fig. 1. Homology models of (**A**) OCT1 and (**B**) OCT2 based on the X-ray diffraction structure for Sugar Transport Protein 10 of *Arabidopsis thaliana* (PDB ID 6H7D) and computational dockings of (*R,R*)-fenoterol (yellow) and (*S,S*)-fenoterol (green). Shown in cyan are the respective fenoterol enantiomers in their putative binding conformations that were used for molecular dynamics simulations and detailed analysis.

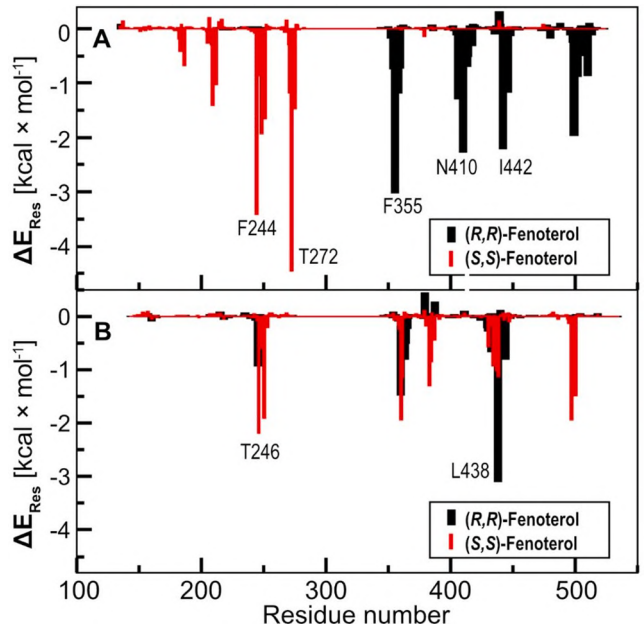

Fig. 2. Decomposition analysis showing the putative residue-wise contributions to the total binding free energies for both fenoterol enantiomers to (**A**) OCT1 and (**B**) OCT2.

Table 4
Key residues that most strongly contribute to the interactions with both fenoterol enantiomers in OCT1 and OCT2. Their individual binding free energies are shown in parentheses. Residues selected for site-directed mutagenesis are highlighted in bold.

	Binding free energy [kcal/mol]	
	OCT1	**OCT2**
(*R*,*R*)-fenoterol	**PHE355** (−3.0 kcal/mol) SER358 (−1.2 kcal/mol) MET406 (−1.3 kcal/mol) SER409 (−1.2 kcal/mol) **ASN410** (−2.3 kcal/mol) **ILE442** (−2.2 kcal/mol) ILE446 (−1.2 kcal/mol)	**LEU438** (−3.1 kcal/mol)
(*S*,*S*)-fenoterol	GLN209 (−1.4 kcal/mol) VAL212 (−1.0 kcal/mol) **PHE244** (−3.4 kcal/mol) LEU248 (−1.9 kcal/mol) LEU251 (−1.7 kcal/mol) PRO271 (−1.2 kcal/mol) **THR272** (−4.5 kcal/mol) PHE275 (−1.5 kcal/mol)	**THR246** (−2.2 kcal/mol) LEU250 (−1.9 kcal/mol) SER383 (−1.3 kcal/mol) CYS437 (−1.0 kcal/mol) LEU438 (−1.1 kcal/mol) LEU497 (−1.9 kcal/mol) VAL499(−1.3 kcal/mol) PHE500 (−1.5 kcal/mol)

considered for preparing input files for subsequent molecular dynamics simulations. The charges were computed for the binding pose geometry of the ligands by using the B3LYP/6-31G* level of theory. The general AMBER force field (GAFF) was used for ligands while FF99SB was used for proteins. Water solvent was described using TIP3P solvent. A sufficient number of counter ions were added to neutralise the systems. The simulations included a minimisation run, constant volume ensemble simulation, and simulation in isothermal-isobaric ensemble. Following an equilibration run for a time scale of 2 ns, the production runs were carried out for 50 ns. The binding free energies were computed using molecular mechanics-generalised Born surface area approach for the 2500 configurations corresponding to 5 ns time scale at the end of the production run. The binding free energies were computed for both enantiomers in different binding sites and the relative binding affinities were discussed based on the results corresponding to high affinity binding sites.

2.3. Site-directed mutagenesis

Point mutations were introduced into the coding sequences of human OCT1 and OCT2 cloned into the pcDNA3.1 vector using the complementary primers listed in Table 1. To avoid primer-primer annealing, a protocol of site-directed mutagenesis using two single-primer reactions in parallel was used [27]. For this, two polymerase chain reactions (PCRs) consisting of 6.25 µl DNA (80 ng/µl), 5 µl Q-solution (Qiagen, Hilden, Germany), 2.5 µl 10 × KOD buffer (KOD Hot Start DNA Polymerase Kit; Merck, Darmstadt, Germany), 2.5 µl dNTPs (2 mM each; Thermo Fisher Scientific, Darmstadt, Germany), 1 µl $MgSO_4$ (25 mM; Merck, Darmstadt, Germany), 0.65 µl either forward or reverse primer (10 µM; Sigma-Aldrich, Darmstadt, Germany), 0.5 µl HotStart KOD Polymerase (KOD Hot Start DNA Polymerase Kit; Merck, Darmstadt, Germany) and 6.6 µl twice-distilled water were carried out in parallel at 95 °C for 3 min, followed by 30 cycles at 95 °C for 30 s, 66 °C for 30 s, 72 °C for 4 min, and a final step at 72 °C for 10 min. After this, both PCR mixtures were combined and the DNA was denatured at 95 °C for 5 min, followed by a gradual cooling procedure at 90 °C for 1 min, 80 °C for 1 min, 70 °C for 30 s, 60 °C for 30 s, 50 °C for 30 s, and 40 °C for 30 s. Subsequently, the template DNA was digested using DpnI in a reaction mixture consisting of 6 µl of cut smart buffer (New England Biolabs, Frankfurt am Main, Germany), 3 µl of DpnI (20 U/µl, New England Biolabs), and 50 µl of the PCR product. This was incubated at 37 °C overnight, subsequently dialysed, and then transformed into OneShot TOP10 Electrocomp *E. coli* using an Electroporator Gene Pulser II (Bio-Rad Laboratories, Hercules, California, USA). The entire reading frame of the OCT1 and OCT2 genes were sequenced to confirm successful mutation. The mutated transporter sequence was then cloned into the pcDNA5/FRT expression vector (Thermo Fisher Scientific, Darmstadt, Germany) and used for the stable transfection of human embryonic kidney (HEK)293 T-REx cells.

2.4. Stable transfection of wild-type and mutated OCT1- and OCT2-overexpressing cell lines

HEK293 T-REx cells overexpressing the WT or mutated sequences of human OCT1 and OCT2 were cultured in Dulbecco's modified Eagle's medium (DMEM) supplemented with 10% foetal calf serum (FCS), penicillin (100 U/ml), and streptomycin (100 µg/ml; all obtained from Thermo Fisher Scientific, Darmstadt, Germany) and incubated at 37 °C, 95% relative humidity, and 5% CO_2.

These cells were generated by targeted chromosomal integration using the Flp-In™ system (Thermo Fisher Scientific, Darmstadt, Germany), as described before [28,29]. Briefly, 10^6 cells were plated in a 6-well plate and, following incubation for 24 h, transfected with both 3.6 µg helper plasmid pOG44 and 400 ng pcDNA5 expression vector. To do so, the cDNA and 12 µl FuGene6 transfection reagent (Promega Corporation, Walldorf, Germany) were each diluted in 100 µl of DMEM, incubated for 5 min at room temperature, mixed together, and incubated again for 15 min. After washing the cells with DMEM supplemented with 10% FCS, 1.8 ml of DMEM with 10% FCS was given to the cells and the 200 µl transfection mixture was added dropwise. Following 24 h of incubation, the cell culture medium was replaced by DMEM supplemented with FCS, penicillin, and streptomycin, as described above. After another incubation period of 24 h, the cells were transferred to a 100 mm petri dish. Selection of successfully transfected cells using hygromycin B (300 µg/ml; Thermo Fisher Scientific, Darmstadt, Germany) was initiated on the next day. After approximately nine days, single colonies were picked and transferred to a 24-well plate to be cultivated at a reduced hygromycin B concentration of 50 µg/ml. After reaching 70% confluence, the cells were transferred to a 6-well plate and later to a T25 culture flask. Upon first passage, 40% of the cells were used to prepare cell pellets for DNA and RNA isolation for cell line validation, as described below.

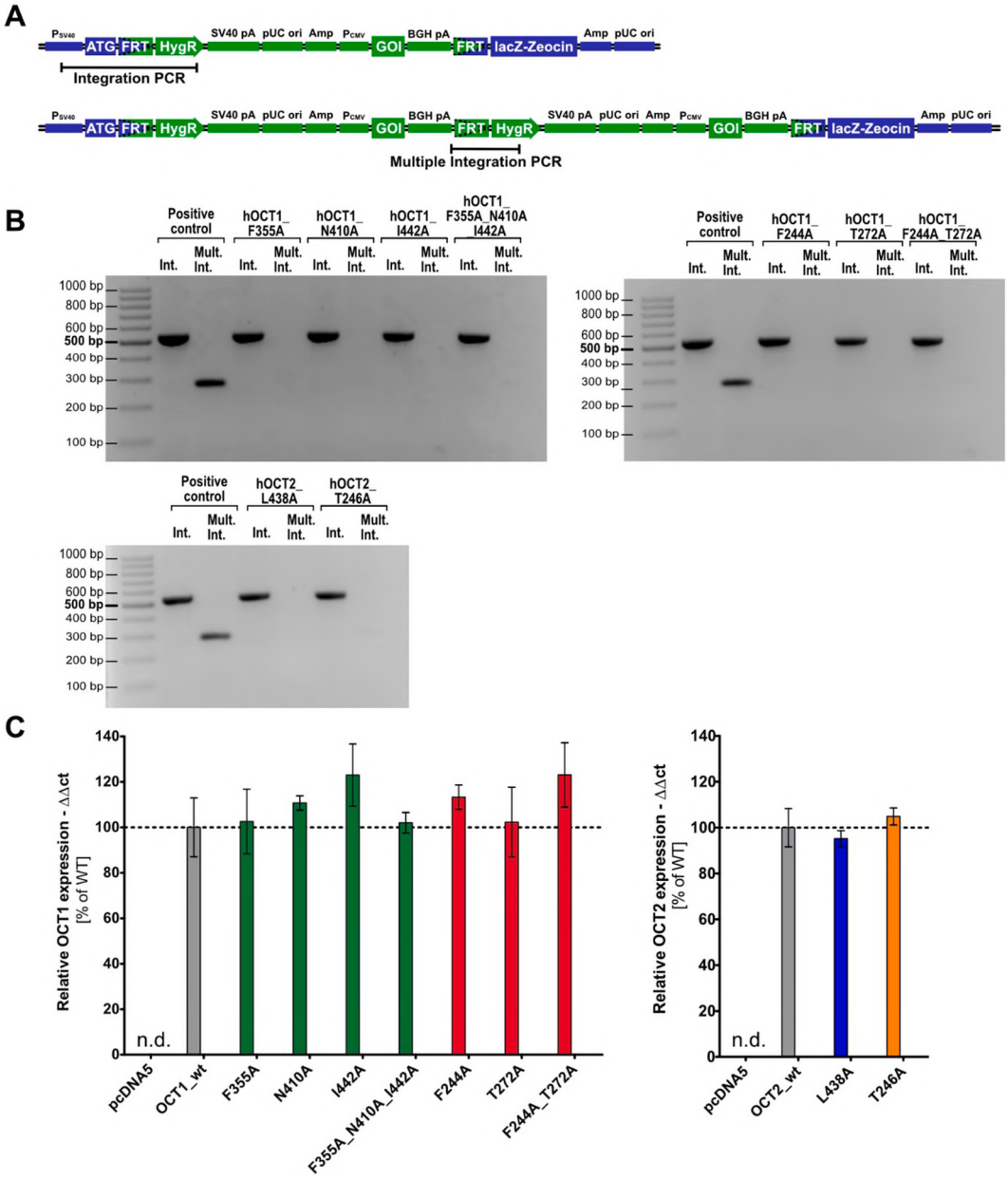

Fig. 3. Validation of generated cell lines overexpressing mutated OCT1 or OCT2 (**A**) Schematic representation of the integrated pcDNA5/FRT expression vector (green) into the host cell genome (blue) for the single and multiple integration. PCRs were carried out to confirm vector integration (integration PCR) and exclude multiple integrations (multiple integration PCR). (**B**) Gel pictures of confirmation PCRs for generated cell lines overexpressing mutated OCT1 or OCT2 (**C**) Expression analysis of mutated transporter-overexpressing cell lines for OCT1 (green) and OCT2 (blue). The gene expression was determined through quantifying the mRNA by real-time PCR and normalised to that of the wild type transporter-overexpressing cell lines. Data is shown as mean ± SEM of 3 independent measurements at different cell passages. N.d., not detectable.

2.5. Genomic validation of generated cell lines

Genomic DNA was isolated using the QIAGEN DNeasy Blood & Tissue Kit (Qiagen, Hilden, Germany), according to the manufacturer protocol. For this, approximately 2×10^6 cells were harvested by centrifugation (400 × g, 5 min, rt) and pellets were either stored at −20 °C or used directly for DNA extraction. The extraction was then performed using the QIACube robot (Qiagen, Hilden, Germany). The stable, genomic integration of the transfected expression vector was validated by integration PCR. A multiple integration PCR was carried out to exclude multiple vector integrations. Both PCR mixtures were composed of 5 µl of 2× QIAGEN Multiplex PCR Master mix (Qiagen, Hilden, Germany), 2 µl Q-Solution (Qiagen), 0.25 µl forward primer (10 µM; Table 1), 0.25 µl reverse primer (10 µM), 1 µl genomic DNA (100 ng), and 1.5 µl twice-distilled water. The PCR protocols were as follows: 95 °C for 15 min, followed by 35 cycles of 95 °C for 30 s, 62.7 °C for 90 s, 72 °C for 90 s, and a final step at 72 °C for 10 min. The genomic DNA of a cell clone which showed multiple integration was used as a positive control for each PCR.

2.6. Quantification of gene expression

Total RNA isolation was carried out using the RNeasy Plus Mini Kit (Qiagen, Hilden, Germany), according to manufacturer's instructions. For this, approximately 2×10^6 cells were harvested by centrifugation (400g, 5 min, rt) and resuspended in 350 µl RLT lysis buffer (Qiagen) supplemented with 1% β-mercaptoethanol (v/v; Sigma-Aldrich, Darmstadt, Germany). Automatic isolation was carried out using the QIACube robot (Qiagen).

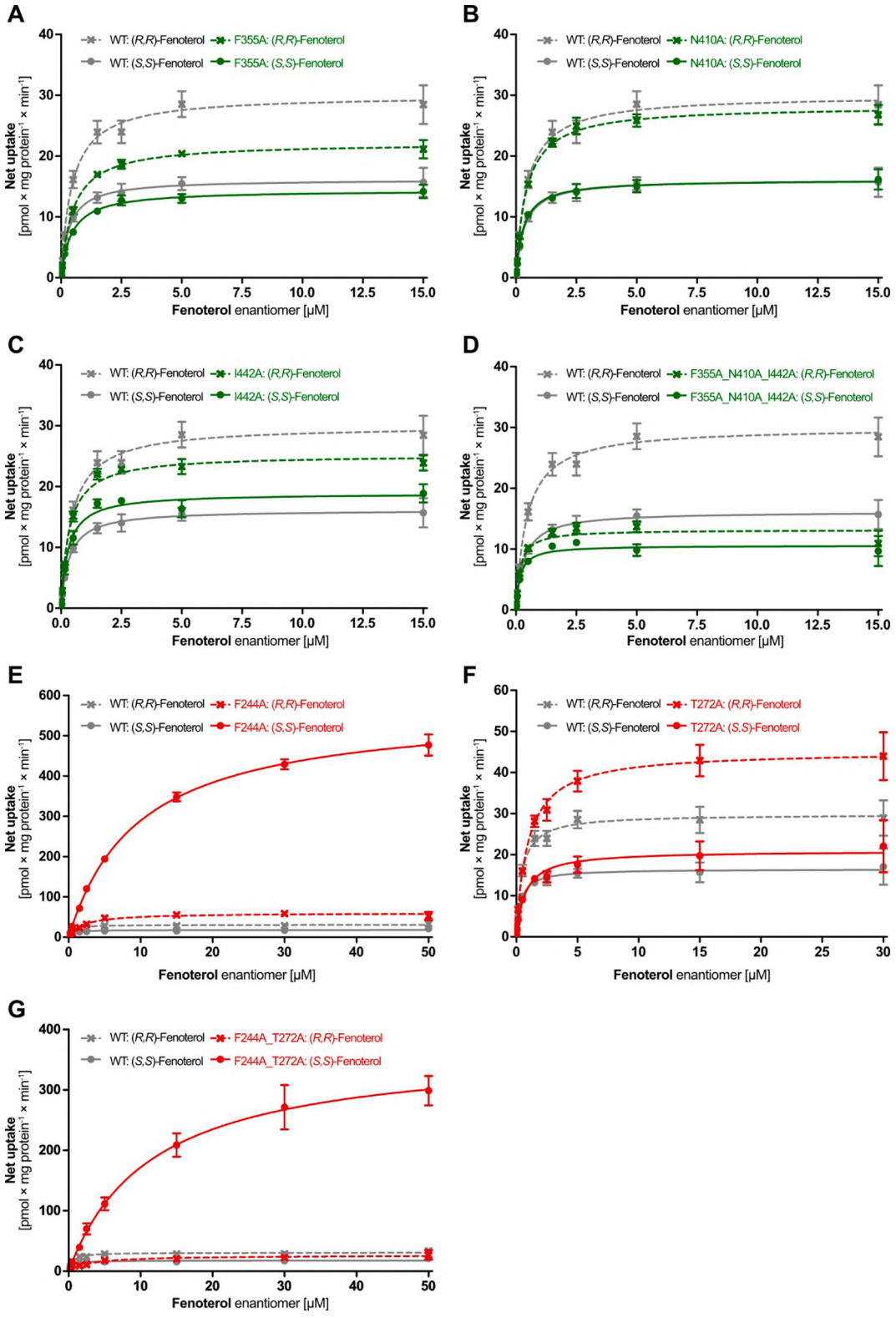

Fig. 4. Stereoselective cell uptake of racemic fenoterol by WT (grey) and mutated (green or red) human OCT1, determined in recombinant HEK293 cells and detected for each fenoterol enantiomer individually using HPLC-MS/MS. The curves for *(R,R)*-fenoterol are shown as dashed lines and those for *(S,S)*-fenoterol as solid lines. The mutations that, according to our computational studies, affect mainly *(R,R)*-fenoterol are shown in green and those that affect mainly *(S,S)*-fenoterol are shown in red. Shown is the net uptake as mean ± S.E.M. of at least 4 independent experiments. The net uptake was calculated as the difference between the cell uptake in transporter-overexpressing cell lines and the uptake in an empty vector-transfected control cell line.

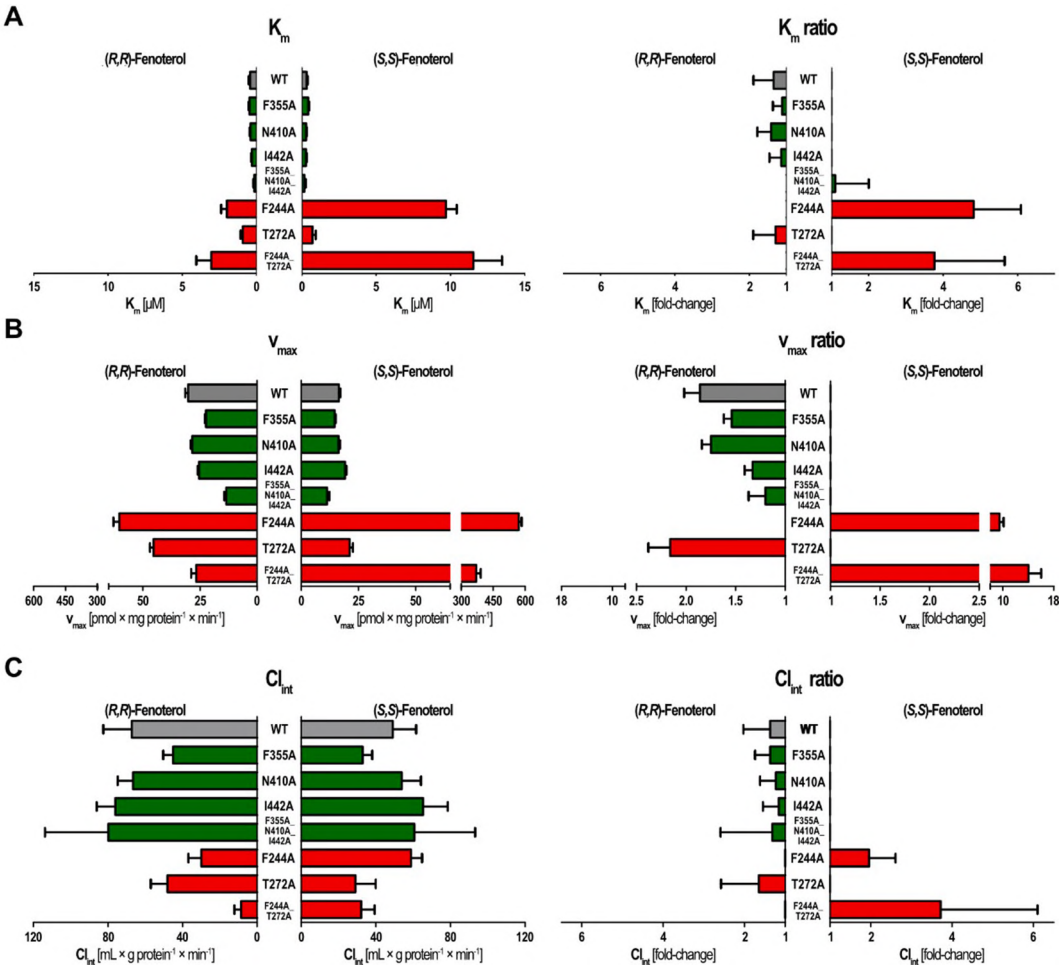

Fig. 5. Stereoselectivity in the cell uptake of racemic fenoterol by WT (grey) and mutated (green/red) human OCT1, shown as absolute values (left) and as ratios (quotient of the higher and the lower values to represent stereoselectivity; right) of the pharmacokinetic parameters. The mutations that, according to our computational studies, affect mainly *(R,R)*-fenoterol are shown in green and those that affect mainly *(S,S)*-fenoterol are shown in red.

Immediately after RNA isolation, cDNA synthesis was performed using the Superscript II Reverse Transcriptase Kit (Thermo Fisher Scientific, Darmstadt, Germany). For this, 3 µg of RNA were diluted in 17.75 µl RNase free water. Subsequently, 1 µl anchored-dT primers (10 µM, 5′-TTTTTTTTTTTTTTTTTVN-3′) were added to initiate primer annealing at 70 °C for 10 min. After this, 11.25 µl of a reverse transcription reaction mixture composed of 6 µl 5× Superscript RT buffer, 3.5 µl dithiothreitol (0.1 M), 1 µl dNTPs (10 mM), 0.5 µl RNase inhibitor P/N (40 U/µl), 0.25 µl SuperScript II reverse transcriptase (200 U/µl) was added and reverse transcription was carried out at 42 °C for 60 min. This was followed by enzyme denaturation at 75 °C for 15 min. The 30 µl synthesised cDNA were diluted by adding 70 µl RNase free water and further diluted 1:10 prior to quantitative real-time PCR.

For the expression analysis of generated cell lines, RNA was isolated from three different passages. For each mutation, gene expression of at least three different cell clones were analysed using the HOT FIREPol EvaGreen qPCR Mix Plus kit (Solis BioDyne, Tartu, Estonia). The reaction mixture was composed of 2 µl 5× EvaGreen qPCR Mix, 5.6 µl twice-distilled H_2O, 0.4 µl primer mixture (10 µM each of forward and reverse primers) and 2 µl cDNA (6 ng). The PCR was carried out in a 384 well-plate using a Taqman 7900 T (Applied Biosystems, Darmstadt, Germany). Each sample was measured in technical triplicates and cycle threshold values were identified using the SDS 1.2 software (Applied Biosystems). Finally, the ΔΔct method [30] was used to determine the relative gene expression according to the following formula:

$$\text{Relative expression} = 2^{-\left(ct_{mutant} - ct_{mutant,HPRT1}\right) - \left(ct_{wt} - ct_{wt,HPRT1}\right)}$$

2.7. *In vitro transport experiments*

Aciclovir, fenoterol, and salbutamol were purchased from Sigma-Aldrich (Darmstadt, Germany; catalogue numbers PHR1254, F1016, and S8260, respectively), fenoterol-d6 from Biozol Diagnostica (Eching, Germany; F248852), and tulobuterol from Santa Cruz Biotechnology (Darmstadt, Germany; sc-213131). According to the respective manufacturers, all test compounds were > 95% pure. For cellular uptake experiments, 600,000 cells were plated in 12-well plates pre-coated with poly-D-lysine and incubated for 48 h. The transport experiments were carried out at 37 °C. All cells were washed once with pre-warmed (37 °C) HBSS+ (10 mM HEPES in Hank's balanced salt solution (HBSS), pH 7.4; Thermo Fisher Scientific, Darmstadt, Germany) and incubated with the pre-warmed substrate in HBSS+ at 37 °C for exactly 2 min. The rate of fenoterol uptake by OCT1 was previously determined to be linear for 10 min [6]. It was assumed to be linear for OCT2 as well, based on previous experience with this expression system. Cell uptake was stopped by washing the cells twice with ice-cold HBSS+. The cells were subsequently lysed using 80% acetonitrile (LGC Standards, Wesel, Germany) containing fenoterol-d6 (50 ng/ml) as internal standard for high performance liquid chromatography coupled to tandem mass spectrometry (HPLC-MS/MS) analysis. Additionally, two wells per cell line were lysed using RIPA buffer and total protein was quantified by comparison to a

Table 5
Kinetic parameters for the transport of racemic fenoterol by WT and mutated OCT1.

Mutation	Substrate	K_m ± S.E.M. [μM]	V_{max} ± S.E.M. [pmol × mg protein^{-1} × min^{-1}]	Cl_{int} ± S.E.M. [mL × g protein^{-1} × min^{-1}]	Stereoselectivity		
					K_m	V_{max}	Cl_{Int}
WT	*(R,R)*-Fenoterol	0.46 ± 0.08	30.0*** ± 1.2	67.3 ± 15.3	1.39-fold	1.85-fold	1.37-fold
	(S,S)-Fenoterol	0.33 ± 0.07	16.2*** ± 0.7	49.0 ± 12.7	for *(R,R)*	for(*R,R*)	for *(R,R)*
F355A	*(R,R)*-Fenoterol	0.49 ± 0.05	22.2*** ± 0.5	45.1 ± 5.3	1.11-fold	1.54-fold	1.37-fold
	(S,S)-Fenoterol	0.44 ± 0.06	14.4*** ± 0.4	32.9 ± 5.1	for *(R,R)*	for *(R,R)*	for *(R,R)*
N410A	*(R,R)*-Fenoterol	0.42 ± 0.04	28.2*** ± 0.6	66.6 ± 8.2	1.40-fold	1.75-fold	1.23-fold
	(S,S)-Fenoterol	0.30 ± 0.05	16.1*** ± 0.5	54.0 ± 10.3	for *(R,R)*	for *(R,R)*	for *(R,R)*
I442A	*(R,R)*-Fenoterol	0.33 ± 0.04	25.2*** ± 0.6	76.1 ± 10.0	1.14-fold	1.33-fold	5.21-fold
	(S,S)-Fenoterol	0.29 ± 0.05	18.9*** ± 0.7	65.35 ± 13.17	for *(R,R)*	for *(R,R)*	for *(R,R)*
F355A_N410A_I442A	*(R,R)*-Fenoterol	0.16 ± 0.17	13.3 ± 0.8	79.9 ± 33.9	1.13-fold	1.20-fold	1.32-fold
	(S,S)-Fenoterol	0.18 ± 0.08	11.1 ± 0.9	60.7 ± 32.5	for *(S,S)*	for *(R,R)*	for *(R,R)*
F244A	*(R,R)*-Fenoterol	2.64*** ± 0.38	60.2*** ± 2.6	30.0* ± 6.9	3.67-fold	9.44-fold	1.95-fold
					for *(S,S)*	for *(S,S)*	for *(S,S)*
	(S,S)-Fenoterol	9.68*** ± 0.73	568*** ± 14	58.6* ± 5.9			
T272A	*(R,R)*-Fenoterol	0.94 ± 0.14	45.2*** ± 1.6	48.1 ± 8.9	1.31-fold	2.16-fold	1.65-fold
	(S,S)-Fenoterol	0.72 ± 0.22	20.9*** ± 1.4	29.1 ± 10.9	for *(R,R)*	for *(R,R)*	for *(R,R)*
F244A_T272A	*(R,R)*-Fenoterol	3.06** ± 1.01	26.4*** ± 2.2	8.6* ± 3.6	3.76-fold	14.0-fold	3.73-fold
					for *(S,S)*	for *(S,S)*	for *(S,S)*
	(S,S)-Fenoterol	11.5** ± 1.9	370*** ± 21	32.1* ± 7.2			

S.E.M., standard error of the mean; asterisks indicate statistical significance of the differences between the two enantiomers (Student's *t*-test; *p < 0.05, **p < 0.01, ***p < 0.001).

standard curve using bovine serum albumin (Sigma-Aldrich, Darmstadt, Germany) in a bichinonic acid assay [31]. This was later used for the normalisation of cellular uptake to the density of seeded cells.

2.8. Liquid chromatography and mass spectrometric detection

Cellular uptake of test compounds was quantified by HPLC-MS/MS using a Shimadzu Nexera HPLC system with a LC-30AD pump, a SIL-30AC autosampler, a CTO-20AC column oven, and a CBM-20A controller (all Shimadzu, Kyoto, Japan). Detection was done by an API 4000 tandem mass spectrometer (AB SCIEX, Darmstadt, Germany) operating in the multiple reaction monitoring mode. The corresponding detection parameters are listed in Table 2. Peak detection was done using the Analyst 1.6.2 software (AB SCIEX, Darmstadt, Germany) and quantified by the simultaneous measurement of standard curves with known concentrations.

Chiral separation of fenoterol enantiomers was done using a CHIRALPAK CBH HPLC column (100 × 3 mm, 5 μm; Sigma-Aldrich, Darmstadt, Germany) with a corresponding 10 × 3 mm guard column. HPLC was carried out with a flow rate of 500 μl/min and an oven temperature of 22 °C. The aqueous mobile phase was buffered with 10 mM ammonium acetate (pH adjusted to 5.8; Merck, Darmstadt, Germany) and supplemented with 5% (v/v) isopropyl alcohol as organic modifier. The order of elution of the fenoterol enantiomers was obtained from available literature [32].

Chiral salbutamol separation was done on an Astec Chiriobiotic T column (15 cm × 2.1 mm, 5 μm; Sigma-Aldrich, Darmstadt, Germany) with a corresponding 2 cm × 1 mm guard column. Oven temperature was 25 °C and flow rate was set to 700 μl/min. The mobile phase was composed of 20 mM ammonium acetate (pH adjusted to 4.5; Merck, Darmstadt, Germany) supplemented with 95% (v/v) methanol (Promochem, Wesel, Germany). The order of elution was also obtained from reference literature [33].

2.9. Calculations

Cellular uptake was normalised to the total protein quantity and transporter-mediated net uptake was calculated by subtracting the uptake measured in an empty-vector transfected control cell line from the uptake of transporter-overexpressing cells. The kinetic parameters K_m and v_{max} were estimated by non-liner regression according to the Michaelis-Menten equation using GraphPad Prism 5.01 (GraphPad Software, La Jolla, CA, United States). The intrinsic clearance Cl_{int} was calculated by dividing v_{max} by K_m. Uptake ratios were calculated by

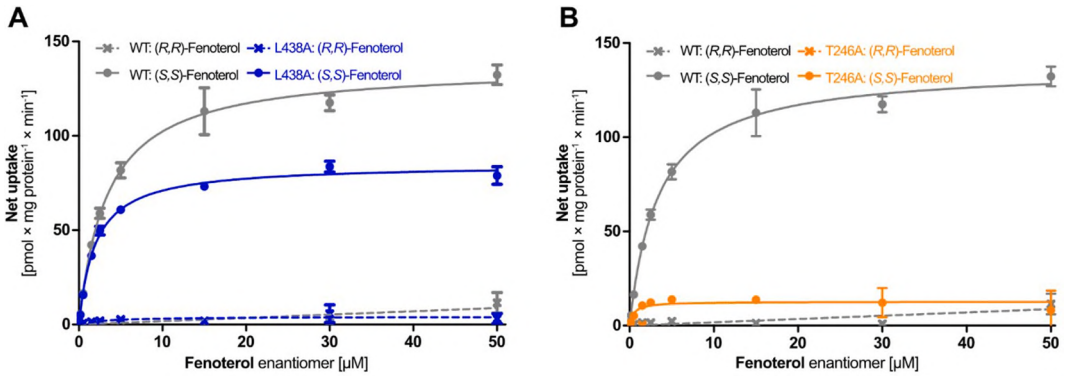

Fig. 6. Stereoselective cell uptake of racemic fenoterol by WT (grey) and mutated (blue or orange) human OCT2, determined in recombinant HEK293 cells and detected for each fenoterol enantiomer individually using HPLC-MS/MS. The curves for *(R,R)*-fenoterol are shown as dashed lines and those for *(S,S)*-fenoterol as solid lines. The mutation that, according to the computational studies, affects mainly *(R,R)*-fenoterol is shown in (**A**) and in blue and that which affects mainly *(S,S)*-fenoterol is shown in (**B**) and in orange. Shown is the net uptake as mean ± S.E.M. of at least 4 independent experiments. The net uptake was calculated as the difference between the cell uptake in transporter-overexpressing cell lines and the uptake in an empty vector-transfected control cell line.

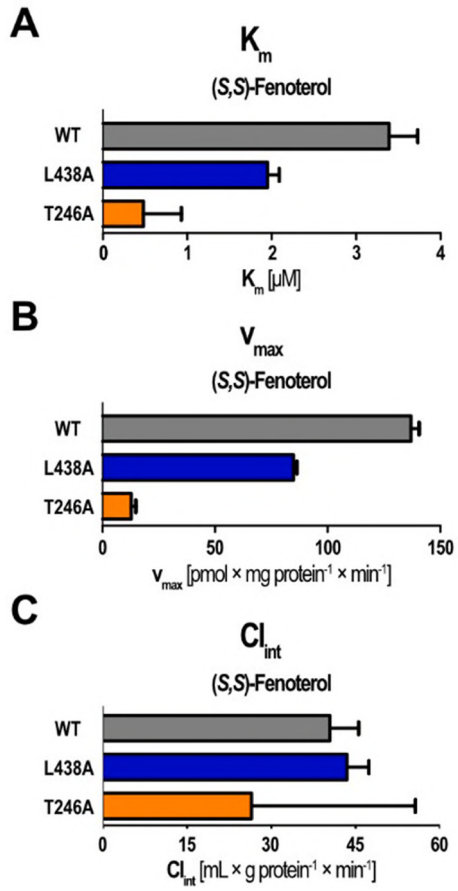

Fig. 7. Graphical representation of the pharmacokinetic parameters pertaining to the cell uptake of racemic fenoterol by WT (grey) and mutated (blue/orange) human OCT2. As (*R,R*)-fenoterol showed zero specific uptake, ratios representing the stereoselectivity could not be calculated. The mutation that, according to the computational studies, affects mainly (*R,R*)-fenoterol is shown in blue and that which affects mainly (*S,S*)-fenoterol is shown in orange.

Table 6
Kinetic parameters for the transport of racemic fenoterol by WT and mutated OCT2.

Mutation	Substrate	K_m ± S.E.M. [μM]	V_{max} ± S.E.M. [pmol × mg protein^{-1} × min^{-1}]	Cl_{int} ± S.E.M. [mL × g protein^{-1} × min^{-1}]
WT	*(R,R)*-Fenoterol	No specific transport[a]		
	(S,S)-Fenoterol	3.39 ± 0.34	137 ± 3.6	40.4 ± 5.1
L438A	*(R,R)*-Fenoterol	No specific transport[a]		
	(S,S)-Fenoterol	1.95 ± 0.14	84.8 ± 1.5	43.4 ± 3.9
T246A	*(R,R)*-Fenoterol	No specific transport[a]		
	(S,S)-Fenoterol	0.48 ± 0.45	12.7 ± 2.1	26.5 ± 29.2

[a] Kinetic parameters could not be calculated for (*R,R*)-fenoterol, as no OCT2-mediated transport was seen in the cellular uptake assays. Stereoselectivity calculations were thus not possible.

dividing cellular uptake of transporter-overexpressing cell lines by the uptake in empty-vector control cells.

3. Results

3.1. Homology models of OCT1 and OCT2 and docking of fenoterol enantiomers

The homology models for OCT1 and OCT2 developed in this study were found to be reliable, as 96% of the residues resided in the allowed regions of the Ramachandran plot (not shown). About 1.6% of the residues were found to be outliers. The structures were used for molecular docking as such without any further modification. Multiple binding modes were obtained for both fenoterol enantiomers in both OCT1 and OCT2. However, only the selected high affinity binding modes were considered for molecular dynamics simulations, as it would be computationally very demanding to carry out molecular dynamics simulations for all the binding modes. Moreover, the equilibrium structures are dominated by high affinity binding modes. Thus, our approach here provides a reasonable approximation. In the case of OCT1, both enantiomers occupy distinct binding sites while in OCT2, the binding site was the same (Fig. 1). Both enantiomers can adopt a fully stretched or a closed conformation. In OCT1, (*R,R*)-fenoterol adopted an extended conformation while (*S,S*)-fenoterol adopted a closed conformation. As for OCT2, a rather reverse trend was observed. The conformational selection was based on the binding site microenvironment and cavity volumes. The substrates adopted a conformation in a way as to maximise the electrostatic and hydrophobic interactions with the residues in the target binding sites.

In addition, binding free energy calculations were carried out for the two enantiomers with both OCT1 and OCT2 (Table 3). According to these, OCT1 showed preferential binding to (*R,R*)-fenoterol (ΔG = −38.2 kcal/mol) over the (*S,S*)-enantiomer (ΔG = −25.9 kcal/mol). Again, the opposite was observed in OCT2, which showed preferential binding for (*S,S*)-fenoterol (ΔG = −30.0 kcal/mol) over the (*R,R*)-counterpart (ΔG = −15.5 kcal/mol). This correlates well with previously reported experimental data, where a 2-fold higher v_{max} was observed in in vitro transport assays for (*R,R*)- over (*S,S*)-fenoterol in OCT1 and a 20-fold higher v_{max} was observed for (*S,S*)- over (*R,R*)-fenoterol in OCT2 [7].

For a better understanding of the enantiopreference of OCT1 and OCT2, a decomposition analysis was done to determine residue-wise contributions to the total binding free energies (Fig. 2). Moreover, it was aimed at identifying the key residues involved in the enantiopreference to be selected for site-directed mutagenesis. With respect to OCT1, both enantiomers bound to distinct binding sites, and the residue-wise contributions mostly came from later residues with residue numbers above 350 for (*R,R*)-fenoterol, while the contributions were mainly from earlier residues with residue numbers below 300 for the (*S,S*)-enantiomer. The decomposition analysis plot (Fig. 2) showed four major peaks for each enantiomer, as they are mainly interacting with four helices in OCT1. In contrast, both fenoterol enantiomers interact with five helices in OCT2, as indicated by five main peaks in the decomposition analysis plot. The key residues that strongly contribute to the binding free energies are listed in Table 4. The residues with the highest contributions were selected for site-directed mutagenesis and studied in more detail.

3.2. Site-directed mutagenesis

The residues that were predicted, based on the residue-wise decomposition analysis, to interact most strongly with each fenoterol enantiomer were substituted individually and in combination by alanine in the open reading frames of human OCT1 and OCT2 by site-directed mutagenesis. For OCT1, the mutated residues were PHE355, ASN410, and ILE442 for studying the interaction with (*R,R*)-fenoterol as well as

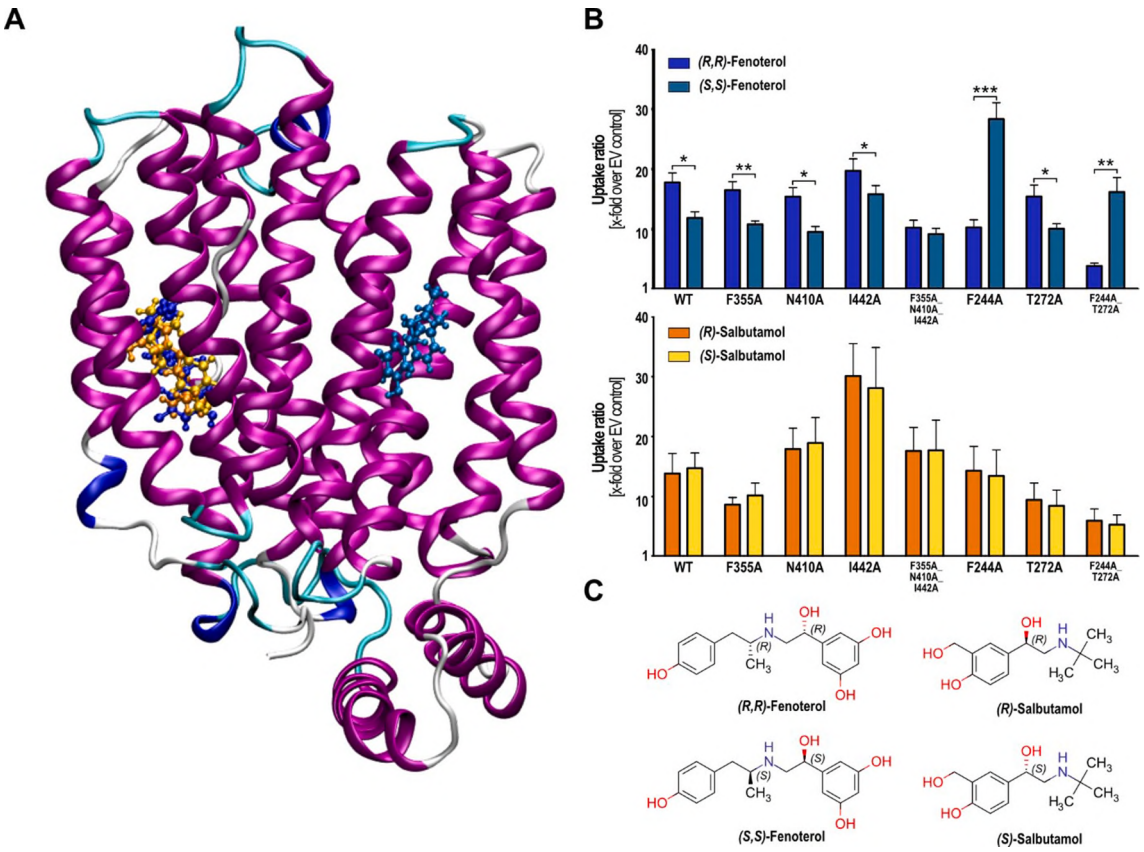

Fig. 8. (**A**) Computational docking of (*R*)-salbutamol (dark orange) and (*S*)-salbutamol (light orange) in the OCT1 homology model. For comparison, (*R,R*)-fenoterol (light blue) and (*S,S*)-fenoterol (dark blue) are also shown. (**B**) In vitro transport of the aforementioned compounds at a single concentration of 1 μM (fenoterol) and 2.5 μM (salbutamol) in WT and mutated OCT1-overexpressing cells. Shown are the ratios of the cellular uptake in transporter-overexpressing cells and empty vector (EV) control cells, calculated using the means of 3 independent experiments. The statistical significance of differences between enantiomers as well as between WT and mutated OCT1 was determined using Student's *t*-test (*$p < 0.05$, **$p < 0.01$, ***$p < 0.001$). For (*R,R*)-fenoterol, differences compared to WT were significant for F244A, the double mutant, and the triple mutant. For (*S,S*)-fenoterol, this was the case for I442A and F244A. Any differences between (*R*)- and (*S*)-salbutamol as well as between WT and mutation were not statistically significant. (**C**) Two-dimensional structures of both fenoterol and salbutamol enantiomers.

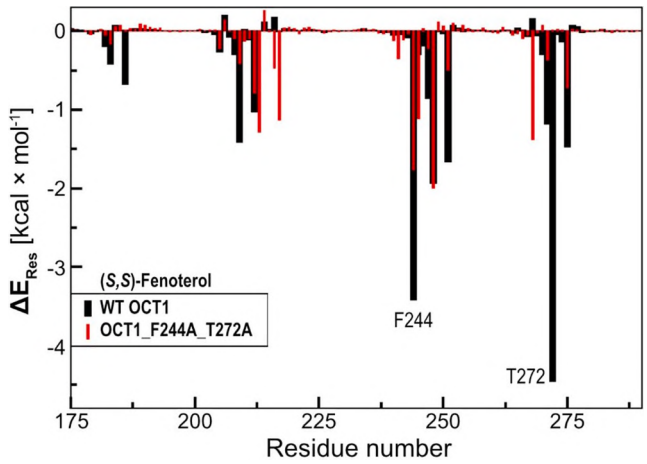

Fig. 9. Decomposition analysis showing the putative residue-wise contributions to the total binding free energies for (*S,S*)-fenoterol to WT OCT1 (black) and OCT1_F244A_T272A (red).

PHE244 and THR272 for (*S,S*)-fenoterol. For OCT2, the mutated residues were LEU438 for (*R,R*)-fenoterol and THR246 for (*S,S*)-fenoterol. Cell lines stably overexpressing the mutated transporters were generated using the Flp-In™ system, after which the genomic integration of the expression vector was confirmed by PCR and the absence of multiple integrated plasmids was verified by another PCR (Fig. 3A and B). Using quantitative PCR, the amount of mRNA was quantified and the gene expression thereby found to be relatively similar for all of the generated cell lines (Fig. 3C).

3.3. *Transport kinetics assessment of OCT1 mutants*

In order to confirm the predicted strong interactions between fenoterol enantiomers and selected residues, the effect of mutating these was assessed in vitro. To this end, cell uptake of fenoterol was determined in cell lines overexpressing the mutated transporters and compared to the wild-type (WT) transporters.

A 1.9-fold higher v_{max} and a slightly lower affinity (1.4-fold higher K_m) for the (*R,R*)-enantiomer of fenoterol compared to (*S,S*)-fenoterol was observed in WT OCT1 (Fig. 4, Fig. 5, Table 5). The v_{max} was only 1.5-fold higher for (*R,R*)-fenoterol and the difference in K_m between both enantiomers almost abolished in the F355A mutant, while the I442A mutation led to a stronger reduction in the difference in v_{max} (merely 1.3-fold higher for (*R,R*)-fenoterol) and a similar effect on the K_m. The observed modest reductions in stereoselectivity by these individual mutations are in line with the predictions that F355 and I442 interact with (*R,R*)- but not with (*S,S*)-fenoterol. In contrast, no significant difference to WT OCT1 was observed for the N410A mutation. When combining these three mutations, stereoselectivity was almost completely abolished, as the v_{max} was then only 1.2-fold higher for (*R,R*)-fenoterol and the K_m 1.1-fold higher for (*S,S*)-fenoterol. A strongly reduced transport for both enantiomers was also observed, as the v_{max}

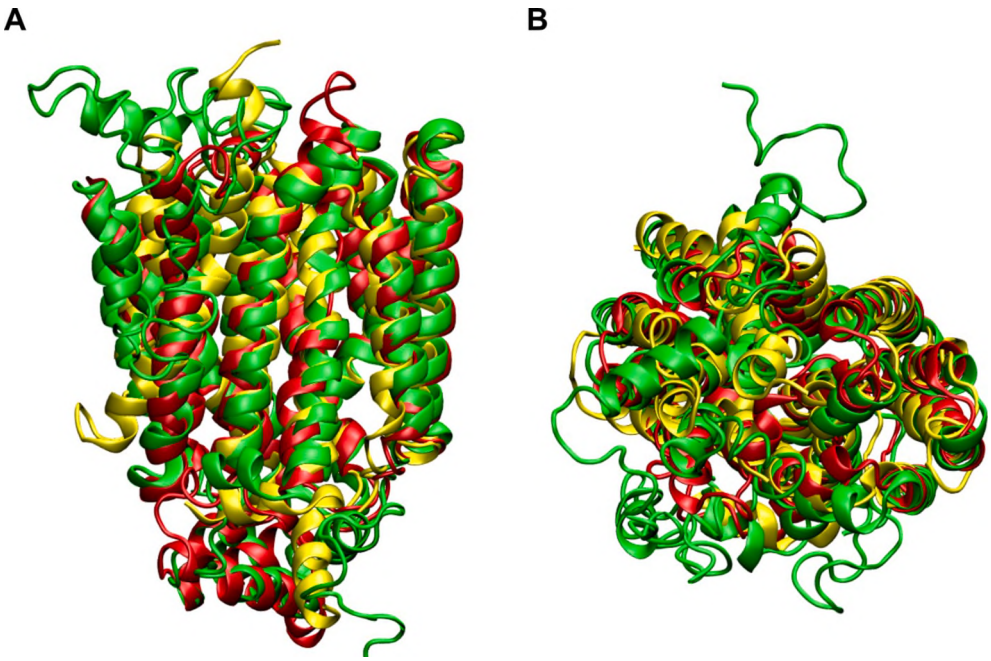

Fig. 10. Structural similarity between the OCT1 homology model created in this study (red) and those previously published by Chen et al. (yellow) and Dakal et al. (green), depicted (**A**) from the side (i.e. from within the cell membrane) and (**B**) from the extracellular space.

was reduced by 56% and 31% for (*R,R*)- and (*S,S*)-fenoterol, respectively, compared to the WT.

With respect to F244A, a 35-fold increase in v_{max} for (*S,S*)-fenoterol compared to WT OCT1 but only a 2.0-fold increase in v_{max} for the (*R,R*)-enantiomer was seen. This resulted in a reversal of the stereoselectivity, as the v_{max} was 9.4-fold higher for (*S,S*)- compared to (*R,R*)-fenoterol in the F244A mutant. While the transport capacity was increased by the F244A mutation, the affinity was reduced, as the K_m was 5.7-fold higher for (*R,R*)-fenoterol and 29-fold higher for (*S,S*)-fenoterol compared to WT OCT1, leading to a 3.7-fold higher K_m (indicating lower affinity) for (*S,S*)- over (*R,R*)-fenoterol. The T272A mutation displayed a slightly higher transport capacity for both fenoterol enantiomers but more strongly for (*R,R*)-fenoterol. As a result, the v_{max} ratio of (*R,R*)- and (*S,S*)-fenoterol was increased to 2.16. F244A and T272A in combination showed similar effects as F244A alone.

3.4. Transport kinetics assessment of OCT2 mutants

While moderate stereoselectivity was observed in fenoterol uptake by OCT1, fenoterol uptake by OCT2 was characterised by complete stereoselectivity, as no net uptake of (*R,R*)-fenoterol was seen in OCT2-overexpressing cells (Fig. 6, Fig. 7, Table 6). The L438A and T246A mutations each led to a reduced v_{max} for (*S,S*)-fenoterol by 38% and 93%, respectively, while the affinity was increased (lower K_m) 1.7-fold and 7.1-fold.

3.5. Comparison between fenoterol and salbutamol in OCT1

To further characterise the putative binding pockets in OCT1, the effects of our mutations on another chiral substrate, salbutamol (also referred to as albuterol), were explored. We had not observed any relevant stereoselectivity in OCT1-mediated cell uptake for this beta-sympathomimetic before [7]. Salbutamol was therefore chosen, so to say, as a counter-example to fenoterol, and both were compared here. Both racemic drugs were tested in vitro at a single concentration (1 μM for fenoterol, 2.5 μM for salbutamol) and the cellular uptake was determined for each enantiomer by chiral HPLC.

For fenoterol, the same key observations as above were seen (Fig. 8B). Namely, an almost twice as high cellular uptake for (*R,R*)- over (*S,S*)-fenoterol, the abolishment of stereoselectivity between both enantiomers in the triple mutant, and the strong increase in uptake of (*S,S*)-fenoterol by F244A. Disparate, however, is the reduction in uptake of (*R,R*)-fenoterol by F244A.

With regard to salbutamol, both enantiomers occupy the same binding site as (*R,R*)-fenoterol (Fig. 8A) according to computational docking in our OCT1 homology model. In line with our previous observations, no statistically significant differences between the enantiomers of salbutamol were observed for WT or any of the mutations (Fig. 8B). For both enantiomers alike, modest effects on cellular uptake were observed for most of the OCT1 mutants. However, these were not statistically significant either.

4. Discussion

In this joint in silico, in vitro, and molecular biological study, the underlying molecular basis for differences in OCT1- and OCT2-mediated transport between fenoterol enantiomers was explored. Based on computational modelling, the enantiopreference for (*R,R*)- over (*S,S*)-fenoterol by OCT1 could possibly be the result of two different binding sites, a concept not implausible in light of the fact that multiple substrate binding sites in OCT1 have been suggested before [8,10–12,14,34]. This hypothesis is supported by our site-directed mutagenesis results, which showed that substituting the residues PHE355 and ILE442, predicted to be most strongly interacting with (*R,R*)-fenoterol, with alanine reduced the v_{max} for (*R,R*)-fenoterol without affecting that of (*S,S*)-fenoterol, and thereby reducing enantiopreference. Individual effects were cumulative, as enantiopreference was almost completely abolished in the triple mutant. In contrast, the predicted relatively strong interaction of (*R,R*)-fenoterol with ASN410 (residue-wise binding free energy = −2.3 kcal/mol) could not be confirmed in vitro, as no significant effects on either the v_{max} or K_m values were observed upon mutation. With respect to the interactions of (*S,S*)-fenoterol with OCT1, the T272A mutation led to a slight increase in the enantiopreference for (*R,R*)-fenoterol, which would have been expected. However, this effect was brought about by increasing the v_{max} for (*R,R*)-fenoterol more strongly than that of (*S,S*)-fenoterol, rather than interfering with the binding of (*S,S*)-fenoterol. Not

entirely conclusive are the results with respect to F244A, where a 35-fold increase in v_{max} for (*S,S*)-fenoterol compared to WT OCT1 was seen. F244 was predicted to be important for the interaction with (*S,S*)-fenoterol, as the residue-wise binding free energy was relatively high (−3.4 kcal/mol). This was reduced to half (Fig. 9) and the overall binding free energy decreased to −19.3 kcal/mol for the OCT1_F244A_T272A double mutant. It was, therefore, expected that mutating F244 would lead to a reduction, not an increase, in the transport of (*S,S*)-fenoterol. However, such a strong effect confirms that F244 is likely to be a key residue for the interaction with (*S,S*)-fenoterol in a different way; in this regard, the predictions were accurate. With regard to OCT2, the 11-fold decrease in v_{max} as a result of the T246A mutation is in accordance with the results from our computational studies, as these had predicted a strong interaction between THR246 and (*S,S*)-fenoterol. L438A was predicted to affect (*R,R*)-fenoterol, but since both enantiomers occupy the same binding region in OCT2, it is not surprising that mutating LEU438 had an effect on the binding of (*S,S*)-fenoterol as well.

The calculated binding free energies (Table 3) are in accordance with the observed enantiopreference for (*R,R*)-fenoterol in OCT1 and for (*S,S*)-fenoterol in OCT2. However, the merely 2-fold difference in the binding free energies for (*R,R*)- and (*S,S*)-fenoterol does not quite reflect the far stronger stereoselectivity observed in vitro, but it is unlikely that these two parameters would correlate perfectly. Replacing some of the key residues had a stronger effect on the K_m of fenoterol transport while other residues mainly affected the v_{max}. While it is evident that the affinity of a substrate, as characterised by the K_m, is determined by the binding energy states, the relationship between binding free energy and v_{max} is less clear. Altogether, it can be concluded that the experimental data compares relatively well with the predictions from computational modelling, and this is another example where in silico and in vitro methods efficiently complement each other.

The main objective of this study was to elucidate the molecular basis for the differential transport of fenoterol enantiomers, which led to the identification of several residues that were shown to be important for fenoterol transport by OCT1. In order to explore whether this might be the case for other substrates as well, another beta-sympathomimetic, salbutamol, was also studied. Both enantiomers were predicted to bind to the same binding site as (*R,R*)-fenoterol. This could possibly explain why – unlike for fenoterol – little to no stereoselectivity (1.12-fold higher v_{max} for (*S*)- over (*R*)-salbutamol, no difference in K_m) was previously observed for salbutamol [7]. Although not entirely conclusive and the effects not strong enough to reach statistical significance, the corresponding in vitro results might somewhat be in line with this, as all of the proposed key residues for (*R,R*)-fenoterol affected salbutamol transport as well. However, it should be kept in mind that salbutamol was only tested at a single concentration (2.5 μM) and the results are, therefore, less reliable.

Other homology models for human OCT1 and OCT2 have previously been reported in the literature. For example, Chen et al. created a homology model for OCT1 by using the X-ray diffraction structure of a phosphate transporter from *Serendipita indica* (PDB ID 4 J05), an endophytic fungus [12]. The resolution of the template structure was 2.9 Å and the transporter was in an inward-facing occluded state with a substrate (phosphate) bound. Dakal and colleagues based their OCT models on the structure of the human glucose transporter GLUT3 (PDB ID 5C65) at a resolution of 2.7 Å [13], while the inward-facing OCT1 model developed by Boxberger et al. used chain A of the glycerol-3-phosphate transporter from *Escherichia coli* at a resolution of 3.3 Å as template (PDB ID 1PW4) [14]. The latter was also used by Zolk and co-workers for their OCT2 model [15]. These models were published before the X-ray diffraction structure for Sugar Transport Protein 10 of *Arabidopsis thaliana* (PDB ID 6H7D), the template used for our OCT1 and OCT2 models, became available. This structure has a higher resolution (2.4 Å) and shows the transporter in the outward occluded state with its substrate glucose bound. As transporter structures in the inward-facing conformation may not yield reliable information about substrate binding, the template chosen here was more suitable for the current study on the stereoselective substrate binding to human OCT1 and OCT2. Furthermore, our OCT1 and OCT2 homology models had 96% of the residues in the allowed region of the Ramachandran plot (not shown), while merely 1.6% of the residues were found to be outliers. Superimposing the OCT1 model created in this study with those reported by Chen et al. and Dakal et al. showed that all three models generally align relatively well (Fig. 10). Substrate recognition and binding by OCTs in general – not with a focus on stereoselectivity – has been studied quite extensively before and several key residues have been proposed [3,35–41]. However, most of this work was conducted using the rat orthologue and other species, and a closer comparison with our results in human OCT1 and OCT2 would become too speculative and is beyond the scope of this study on stereoselectivity.

One key result from this study is that OCT1 may possess distinct binding sites for enantiomers whereas for OCT2, both fenoterol enantiomers appear to bind to the same site. Yet, different enantiomeric binding sites is likely not unique for OCT1. While stereoselective binding to transport proteins has only been scarcely studied so far, some reports for P-glycoprotein (ABCB1), a polyspecific efflux transporter of the ATP-binding cassette transporter family, are found in the literature. The dextrorotatory but not the laevorotatory enantiomer of the antimalarial drug mefloquine was found to compete with cyclosporine A in chromatographic retention experiments. As both mefloquine enantiomers are P-glycoprotein substrates, the authors concluded that (+)-mefloquine may bind, unlike the (−)-enantiomer, to an additional binding site shared by cyclosporine A [42]. A crystal structure of mouse P-glycoprotein showed that the enantiomers of a cyclic hexapeptide inhibitor bind to distinct sites: one binds at the centre of the transporter and the other enantiomer has two binding sites in the upper region of P-glycoprotein [43].

Our work showed that stereoselectivity plays a role in fenoterol transport by OCT1 and, even more so, by OCT2. The clinical implications of these in vitro findings are not yet clear. Fenoterol is mainly excreted as sulphate conjugate and only 2% unchanged in urine [44,45]. Stereoselective transport by OCT1 should thus be more clinically relevant than by OCT2. OCT1 activity was found to determine fenoterol pharmacokinetics in humans [6], but the clinical implications of the 2-fold enantiospecificity was not investigated in this study.

In the absence of an experimentally-determined 3D structure, as is the case for OCT1 and OCT2, the homology modelling and computational docking methodology followed here is a common and well-established approach to derive hypotheses of possible conformations and interactions. However, it should be kept in mind that this merely provides a possible snapshot of a single moment in time for an otherwise highly dynamic system. A more specific limitation to our homology models is the relatively low shared sequence identity of ca. 20% between target proteins and template structure. Previously reported models used different templates but the shared sequence identities were similarly low, as no suitable experimental structures with higher shared sequence identities are available yet. Also, for a better general understanding, it would have been interesting to study a library of structurally closely related synthetic fenoterol derivatives and not only the clinically relevant enantiomers (*R,R*)- and (*S,S*)-fenoterol, but their diastereomers (*R,S*)- and (*S,R*)-fenoterol as well. However, these are not used therapeutically (fenoterol as a drug is a racemic mixture of the (*R,R*)- and (*S,S*)-enantiomers only), and are thus not readily available commercially.

Our work showed that stereoselectivity can play an important role in the transmembranal transport of frequently prescribed drugs, just as it may in receptor binding and enzymatic metabolism. In contrast to these by now well-established concepts, stereoselectivity in drug membrane transport has so far only received very limited attention and is usually not taken into consideration in drug development and therapy. For this to become possible, further research in this field is necessary to arrive at a better understanding of the scope and impact, i.e. the proportion of drugs for which stereoselectivity is observed and how strongly this

affects their pharmacokinetics in a clinical setting. With the experimentally validated and relatively robust OCT1 and OCT2 homology models at hand, reasonable next steps would be to search for other racemic drugs as novel substrates through virtual screenings of large compound databases, computationally predict the importance of stereoselectivity, and confirm (or refute) these findings in vitro.

This study showed – to our knowledge for the first time – that, despite the very close structural similarity, two enantiomers can interact with different and possibly distantly located residues of a transporter. Enantiomers are distinct molecular entities, underlining the necessity to take stereoselectivity in membrane transport and in interactions at membrane transporters into consideration during drug development and therapy. Altogether, the insights gained by this study add to our, as yet, limited understanding on the importance and underlying molecular mechanisms of stereoselectivity in OCT1- and OCT2-mediated cellular uptake as well as on drug transport in general. The homology models of OCT1 and OCT2, corroborated by experimental data, will serve as useful tools for further research on these clinically highly relevant drug transporters.

CRediT authorship contribution statement

Lukas Gebauer: Conceptualization, Investigation, Methodology, Writing – original draft, Writing – review & editing, Visualization. **N. Arul Murugan:** Investigation, Methodology, Writing – original draft, Visualization. **Ole Jensen:** Methodology. **Jürgen Brockmöller:** Conceptualization, Resources, Supervision, Writing – review & editing. **Muhammad Rafehi:** Conceptualization, Funding acquisition, Project administration, Supervision, Writing – original draft, Writing – review & editing, Visualization.

Declaration of Competing Interest

The authors declare that they have no known competing financial interests or personal relationships that could have appeared to influence the work reported in this paper.

Acknowledgements

Funded by the Deutsche Forschungsgemeinschaft (DFG, German Research Foundation) – 437446827 and the research programme of the University Medical Center, University of Göttingen. NAM acknowledges the Swedish Infrastructure Committee (SNIC) for the project “In silico Design of Drugs and Diagnostic Agents for Various Neurodegenerative Diseases” (snic2021-5-1 & 2021-5-39). We would like to thank Ellen Bruns for her excellent technical assistance with the chiral chromatography.

References

[1] Q. Zhou, L.-S. Yu, S. Zeng, Stereoselectivity of chiral drug transport: a focus on enantiomer–transporter interaction, Drug Metab. Rev. 46 (3) (2014) 283–290.
[2] L.A. Nguyen, H. He, C. Pham-Huy, Chiral drugs: an overview, Int. J. Biomed. Sci.: IJBS 2 (2) (2006) 85–100.
[3] H. Koepsell, Organic Cation Transporters in Health and Disease, Pharmacol. Rev. 72 (1) (2020) 253–319.
[4] F. Meyer-Wentrup, U. Karbach, V. Gorboulev, P. Arndt, H. Koepsell, Membrane localization of the electrogenic cation transporter rOCT1 in rat liver, Biochem. Biophys. Res. Commun. 248 (3) (1998) 673–678.
[5] H. Motohashi, Y. Nakao, S. Masuda, T. Katsura, T. Kamba, O. Ogawa, K. Inui, Precise comparison of protein localization among OCT, OAT, and MATE in human kidney, J. Pharm. Sci. 102 (9) (2013) 3302–3308.
[6] M.V. Tzvetkov, J. Matthaei, S. Pojar, F. Faltraco, S. Vogler, T. Prukop, T. Seitz, J. Brockmöller, Increased Systemic Exposure and Stronger Cardiovascular and Metabolic Adverse Reactions to Fenoterol in Individuals with Heritable OCT1 Deficiency, Clin. Pharmacol. Ther. 103 (5) (2018) 868–878.
[7] O. Jensen, M. Rafehi, M.V. Tzvetkov, J. Brockmöller, Stereoselective cell uptake of adrenergic agonists and antagonists by organic cation transporters, Biochem. Pharmacol. 171 (2020), 113731.
[8] R. Moaddel, S. Ravichandran, F. Bighi, R. Yamaguchi, I.W. Wainer, Pharmacophore modelling of stereoselective binding to the human organic cation transporter (hOCT1), Br. J. Pharmacol. 151 (8) (2007) 1305–1314.
[9] T. Seitz, R. Stalmann, N. Dalila, J. Chen, S. Pojar, J.N. Dos Santos Pereira, R. Kratzner, J. Brockmöller, M.V. Tzvetkov, Global genetic analyses reveal strong inter-ethnic variability in the loss of activity of the organic cation transporter OCT1, Genome Med. 7 (1) (2015) 56.
[10] T. Keller, V. Gorboulev, T.D. Mueller, V. Dotsch, F. Bernhard, H. Koepsell, Rat Organic Cation Transporter 1 Contains Three Binding Sites for Substrate 1-Methyl-4-phenylpyridinium per Monomer, Mol. Pharmacol. 95 (2) (2019) 169–182.
[11] H. Koepsell, Multiple binding sites in organic cation transporters require sophisticated procedures to identify interactions of novel drugs, Biol. Chem. 400 (2) (2019) 195–207.
[12] E.C. Chen, N. Khuri, X. Liang, A. Stecula, H.C. Chien, S.W. Yee, Y. Huang, A. Sali, K. M. Giacomini, Discovery of Competitive and Noncompetitive Ligands of the Organic Cation Transporter 1 (OCT1; SLC22A1), J. Med. Chem. 60 (7) (2017) 2685–2696.
[13] T.C. Dakal, R. Kumar, D. Ramotar, Structural modeling of human organic cation transporters, Comput. Biol. Chem. 68 (2017) 153–163.
[14] K.H. Boxberger, B. Hagenbuch, J.N. Lampe, Ligand-dependent modulation of hOCT1 transport reveals discrete ligand binding sites within the substrate translocation channel, Biochem. Pharmacol. 156 (2018) 371–384.
[15] O. Zolk, T.F. Solbach, J. König, M.F. Fromm, Functional characterization of the human organic cation transporter 2 variant p. 270Ala>Ser, Drug Metabolism Disposition: Biol. Fate Chem. 37 (6) (2009) 1312–1318.
[16] P.A. Paulsen, T.F. Custódio, B.P. Pedersen, Crystal structure of the plant symporter STP10 illuminates sugar uptake mechanism in monosaccharide transporter superfamily, Nat. Commun. 10 (1) (2019) 407.
[17] A. Waterhouse, M. Bertoni, S. Bienert, G. Studer, G. Tauriello, R. Gumienny, F. T. Heer, T.A.P. de Beer, C. Rempfer, L. Bordoli, R. Lepore, T. Schwede, SWISS-MODEL: homology modelling of protein structures and complexes, Nucleic Acids Res. 46 (W1) (2018) W296–W303.
[18] UniProt: the universal protein knowledgebase in 2021, Nucleic Acids Res. 49(D1) (2021) D480–D489.
[19] B.P. Pedersen, P.A. Paulsen, T.F. Custodio, Crystal Structure of A. thaliana Sugar Transport Protein 10 in complex with glucose in the outward occluded state, 2018.
[20] O. Trott, A.J. Olson, AutoDock Vina: improving the speed and accuracy of docking with a new scoring function, efficient optimization, and multithreading, J. Comput. Chem. 31 (2) (2010) 455–461.
[21] G. Schaftenaar, J.H. Noordik, Molden: a pre- and post-processing program for molecular and electronic structures*, J. Comput. Aided Mol. Des. 14 (2) (2000) 123–134.
[22] G. Schaftenaar, E. Vlieg, G. Vriend, Molden 2.0: quantum chemistry meets proteins 31(9) (2017) 789-800.
[23] G.W.T.M.J. Frisch, H.B. Schlegel, G.E. Scuseria, M.A. Robb, J.R. Cheeseman, G. Scalmani, V. Barone, G.A. Petersson, H. Nakatsuji, X. Li, M. Caricato, A. Marenich, J. Bloino, B.G. Janesko, R. Gomperts, B. Mennucci, H.P. Hratchian, J.V. Ortiz, A.F. Izmaylov, J.L. Sonnenberg, D. Williams-Young, F. Ding, F. Lipparini, F. Egidi, J. Goings, B. Peng, A. Petrone, T. Henderson, D. Ranasinghe, V.G. Zakrzewski, J. Gao, N. Rega, G. Zheng, W. Liang, M. Hada, M. Ehara, K. Toyota, R. Fukuda, J. Hasegawa, M. Ishida, T. Nakajima, Y. Honda, O. Kitao, H. Nakai, T. Vreven, K. Throssell, J.A. Montgomery Jr., J.E. Peralta, F. Ogliaro, M. Bearpark, J.J. Heyd, E. Brothers, K.N. Kudin, V.N. Staroverov, T. Keith, R. Kobayashi, J. Normand, K. Raghavachari, A. Rendell, J.C. Burant, S.S. Iyengar, J. Tomasi, M. Cossi, J.M. Millam, M. Klene, C. Adamo, R. Cammi, J.W. Ochterski, R.L. Martin, K. Morokuma, O. Farkas, J.B. Foresman, D.J. Fox, Gaussian 09, Revision A.02 (2016).
[24] N.M. O'Boyle, M. Banck, C.A. James, C. Morley, T. Vandermeersch, G. R. Hutchison, Open Babel: An open chemical toolbox, J. Cheminf. 3 (2011) 33.
[25] M.F. Sanner, Python: a programming language for software integration and development, J. Mol. Graph. Model. 17 (1) (1999) 57–61.
[26] G.M. Morris, R. Huey, W. Lindstrom, M.F. Sanner, R.K. Belew, D.S. Goodsell, A. J. Olson, AutoDock4 and AutoDockTools4: Automated docking with selective receptor flexibility, J. Comput. Chem. 30 (16) (2009) 2785–2791.
[27] O. Edelheit, A. Hanukoglu, I. Hanukoglu, Simple and efficient site-directed mutagenesis using two single-primer reactions in parallel to generate mutants for protein structure-function studies, BMC Biotech. 9 (2009) 61.
[28] J.N. Dos Santos Pereira, S. Tadjerpisheh, M. Abu Abed, A.R. Saadatmand, B. Weksler, I.A. Romero, P.O. Couraud, J. Brockmöller, M.V. Tzvetkov, The poorly membrane permeable antipsychotic drugs amisulpride and sulpiride are substrates of the organic cation transporters from the SLC22 family, AAPS J. 16 (6) (2014) 1247–1258.
[29] A.R. Saadatmand, S. Tadjerpisheh, J. Brockmöller, M.V. Tzvetkov, The prototypic pharmacogenetic drug debrisoquine is a substrate of the genetically polymorphic organic cation transporter OCT1, Biochem. Pharmacol. 83 (10) (2012) 1427–1434.
[30] K.J. Livak, T.D. Schmittgen, Analysis of relative gene expression data using real-time quantitative PCR and the 2(-Delta Delta C(T)) Method, Methods (San Diego, Calif.) 25 (4) (2001) 402–408.
[31] P.K. Smith, R.I. Krohn, G.T. Hermanson, A.K. Mallia, F.H. Gartner, M. D. Provenzano, E.K. Fujimoto, N.M. Goeke, B.J. Olson, D.C. Klenk, Measurement of protein using bicinchoninic acid, Anal. Biochem. 150 (1) (1985) 76–85.
[32] M. Sanghvi, A. Ramamoorthy, J. Strait, I.W. Wainer, R. Moaddel, Development and validation of a sensitive LC-MS/MS method for the determination of fenoterol in human plasma and urine samples, J. Chromatogr. B, Analy. Technol. Biomed. Life Sci. 933 (2013) 37–43.

[33] A. Halabi, C. Ferrayoli, M. Palacio, V. Dabbene, S. Palacios, Validation of a chiral HPLC assay for (R)-salbutamol sulfate, J. Pharm. Biomed. Anal. 34 (1) (2004) 45–51.
[34] G. Ciarimboli, K. Struwe, P. Arndt, V. Gorboulev, H. Koepsell, E. Schlatter, J. R. Hirsch, Regulation of the human organic cation transporter hOCT1, J. Cell. Physiol. 201 (3) (2004) 420–428.
[35] C. Popp, V. Gorboulev, T.D. Muller, D. Gorbunov, N. Shatskaya, H. Koepsell, Amino acids critical for substrate affinity of rat organic cation transporter 1 line the substrate binding region in a model derived from the tertiary structure of lactose permease, Mol. Pharmacol. 67 (5) (2005) 1600–1611.
[36] X. Zhang, N.V. Shirahatti, D. Mahadevan, S.H. Wright, A conserved glutamate residue in transmembrane helix 10 influences substrate specificity of rabbit OCT2 (SLC22A2), J. Biol. Chem. 280 (41) (2005) 34813–34822.
[37] V. Gorboulev, N. Shatskaya, C. Volk, H. Koepsell, Subtype-specific affinity for corticosterone of rat organic cation transporters rOCT1 and rOCT2 depends on three amino acids within the substrate binding region, Mol. Pharmacol. 67 (5) (2005) 1612–1619.
[38] C. Volk, V. Gorboulev, A. Kotzsch, T.D. Müller, H. Koepsell, Five amino acids in the innermost cavity of the substrate binding cleft of organic cation transporter 1 interact with extracellular and intracellular corticosterone, Mol. Pharmacol. 76 (2) (2009) 275–289.
[39] D. Gorbunov, V. Gorboulev, N. Shatskaya, T. Mueller, E. Bamberg, T. Friedrich, H. Koepsell, High-affinity cation binding to organic cation transporter 1 induces movement of helix 11 and blocks transport after mutations in a modeled interaction domain between two helices, Mol. Pharmacol. 73 (1) (2008) 50–61.
[40] A. Papaluca, D. Ramotar, A novel approach using C. elegans DNA damage-induced apoptosis to characterize the dynamics of uptake transporters for therapeutic drug discoveries, Sci. Rep. 6 (2016) 36026.
[41] V. Gorboulev, C. Volk, P. Arndt, A. Akhoundova, H. Koepsell, Selectivity of the polyspecific cation transporter rOCT1 is changed by mutation of aspartate 475 to glutamate, Mol. Pharmacol. 56 (6) (1999) 1254–1261.
[42] P. Bhatia, M. Kolinski, R. Moaddel, K. Jozwiak, I.W. Wainer, Determination and modelling of stereoselective interactions of ligands with drug transporters: a key dimension in the understanding of drug disposition, Xenobiotica 38 (2008) 656–675.
[43] S.G. Aller, J. Yu, A. Ward, Y. Weng, S. Chittaboina, R. Zhuo, P.M. Harrell, Y. T. Trinh, Q. Zhang, I.L. Urbatsch, G. Chang, Structure of P-glycoprotein reveals a molecular basis for poly-specific drug binding, Science 323 (2009) 1718–1722.
[44] R.C. Heel, R.N. Brogden, T.M. Speight, G.S. Avery, Fenoterol: A review of its pharmacological properties and therapeutic efficacy in asthma, Drugs 15 (1978) 3–32.
[45] N. Svedmyr, Fenoterol: a beta2-adrenergic agonist for use in asthma. Pharmacology, pharmacokinetics, clinical efficacy and adverse effects, Pharmacotherapy 5 (1985) 109–126.